Towards deformable registration for AR in nephrectomy

Anna Morelli[1], Sara Moccia[1,2], Leonardo S. Mattos[2], Giovanni Cordima[3], Ottavio De Cobelli[3,4], Giancarlo Ferrigno[1] and Elena De Momi[1]
[1] Department of Electronics, Information and Bioengineering, Politecnico di Milano, Milan, Italy
[2] Department of Advanced Robotics, Istituto Italiano di Tecnologia, Genoa, Italy
[3] Department of Urology, Istituto Europeo di Oncologia, Milan, Italy
[4] Universita' degli Studi di Milano, Milan, Italy

***Abstract*—Nephrectomy is the main treatment option for renal cancer. Augmented reality (AR) can assist surgeons in minimally-invasive nephrectomy. Here, intra-operative deformable registration for AR is investigated. When tested on kidney phantom, a RMSE reduction of 13% was achieved with the Free Form Deformation (FFD) registration algorithm, overcoming rigid registration approaches (RMSE reduction = 2%). Results suggested that FFD is a good strategy towards AR for minimally invasive nephrectomy.**

***Keywords*—Augmented reality, nephrectomy, deformable registration, free form deformation**

I. INTRODUCTION

Kidney cancer is the 12^{th} most common cancer, with 338,000 new cases diagnosed annually[1]. The most spread kidney tumor is Renal Cell Cancer (RCC), which accounts for 90% of all malignancies of kidney [1]. A Computed-Tomography (CT) slice of a patient with RCC is shown in Fig. 1. RCC is highlighted with the blue circle. RCC main treatment option is nephrectomy [1]. Nephrectomy is traditionally performed in open surgery, which main advantages deal with the possibility to directly see and touch abdominal structures as to recognize them. However, from the patient's side, open surgery brings risks related to bleeding and infection, as well as long recovery time. To overcome these drawbacks, Minimally Invasive Surgery (MIS) has been introduced [2]. In MIS procedures, three or four incisions are made in the patient's abdomen to provide access for surgical instruments and endoscope. MIS leads to proved benefits for the patient such as reduction of bleeding, pain and risk of infection and recovery time [2]. MIS can be also performed through a robotic device (Robotic MIS - RMIS). RMIS potentially increases MIS accuracy and safety, for example through providing surgeon's tremor filtering [3].

The main drawbacks of RMIS are, however, loss of depth perception, limited field of view and lack of tactile feedback [4]. Augmented Reality (AR) has been introduced to overcome the limitation in the vision. Sensitive structures, such as vessels, can be identified in the pre-operative plan [5] and their intra-operative position can be retrieved with AR systems. The robot can be avoided to enter such forbidden structures, e.g. with the implementation of Active-Constraints (AC) control. Intra-operative guidance, rapid identification of relevant structures and reduction of surgeon's cognitive load are among the proved benefits of AR [6].

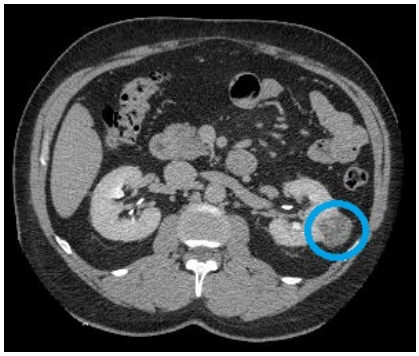

Fig. 1: Renal cell carcinoma (highlighted with the blue circle) in a computer-tomography slice. Courtesy of Istituto Europeo di Oncologia (IEO).

The application of AR in nephrectomy presents non-trivial challenges. With respect to the pre-operative phase, abdominal organs, and in particular kidneys, are intra-operatively deformed by (i) changes in pressure (the patient is insufflated during nephrectomy) and patient's position, (ii) clamping of the renal vessels and (iii) surgeon's organ manipulation and dissection. A recent review on AR system in nephrectomy can be found in [7]. However, the majority of the proposed systems consider the kidney as a rigid body. Other popular approaches model kidney deformation with biomechanical models, with limitations such as high computational cost. A further class of algorithms use intra-operative imaging, such as cone-beam CT, to extract the 3D intra-operative anatomy to be registered with the 3D pre-operative one. However, intra-operative CT brings additional costs and further radiation dose delivered to patients.

In this context, the aim of this work is to investigate the use of deformable registration strategies to tackle intra-operative kidney deformation for accurate and fast AR in nephrectomy without requiring additional imaging instrumentation.

[1]https://www.worldatlas.com/articles/countries-with-the-highest-incidence-of-kidney-cancer-in-the-world.html

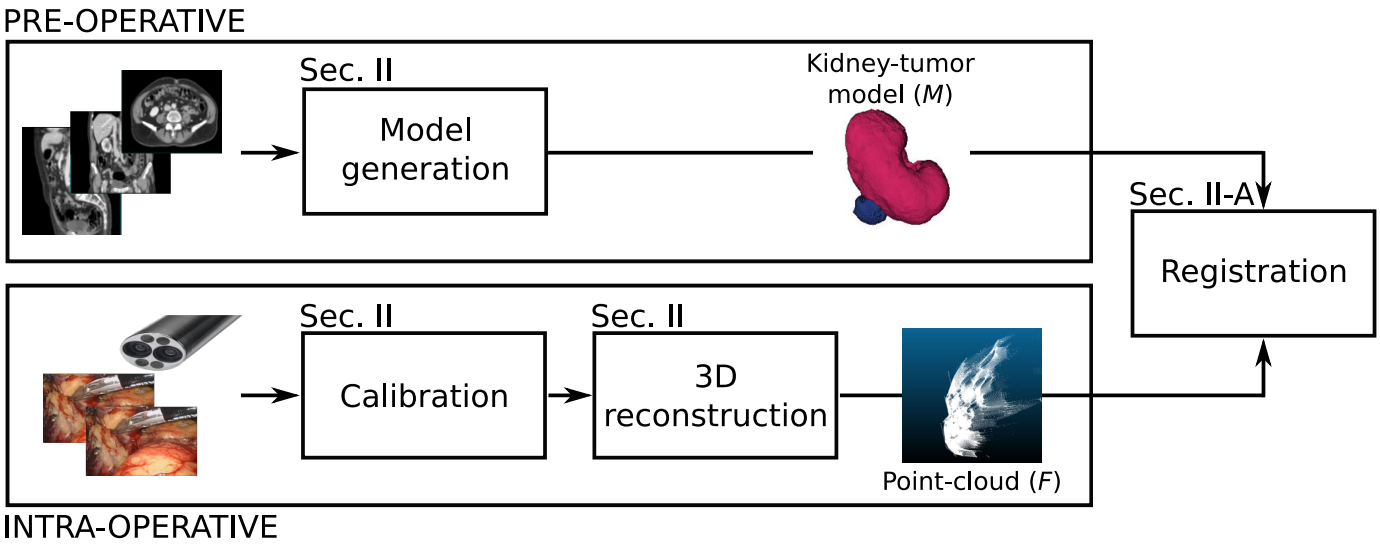

Fig. 2: Proposed workflow for augmented reality in nephrectomy. The pre-operative kidney-tumor model (M) is registered to the intra-operative point cloud (F).

II. Methods

In this section, the proposed approach to register the pre-operative kidney anatomy to the intra-operative scene is explained. The workflow of the approach is shown in Fig. 2. The proposed approach can be split into the following steps:

Model generation To obtain the pre-operative kidney anatomical model, pre-operative abdominal CT slices were segmented with a semiautomatic segmentation method, which exploited deformable-model active contours [8]. From the kidney segmentation mask, the kidney model was obtained with the fast marching method [9]. As a prerequisite for performing intra-operative deformable registration (Sec. II-A), the model vertexes (M) were retrieved. The model generation was implemented in Slicer[2].

Calibration and 3D reconstruction: Intra-operative kidney stereo-images were acquired with the daVinci Research Kit (dVRK)[3] stereocamera (720x576 pixels, 25 Hz, 80 degrees field of view). After camera calibration, performed according to the Zhang calibration method, the intra-operative stereoimages were acquired and dense soft-tissue 3D reconstruction was performed to retrieve the intra-operative 3D point cloud (F) as in [10].

Registration: Deformable registration of M on F was performed with Free Form Deformation (FFD) and B-splines, as described in Sec. II-A

It is worth noting that, for experimental purposes, abdominal phantoms, obtained from real-patients' CT images, were exploited. In particular, kidney-phantom mold was obtained from the kidney model of a real CT image (the model was computed as in **Model generation**). The phantom was then built with polyurethane, according to [11].

[2]https://www.slicer.org/

[3]http://research.intusurg.com/dvrkwiki/index.php?title=Main_Page

A. Deformable registration

The deformable registration exploited in this work is FFD [12]. Indeed, compared with other methods such as thin-plate splines or gaussian mixture model, FFD requires lower computational cost, assures a smoother deformation and allows local control [13], [14], [15].

FFD main idea is to represent the deformation of M as the deformation of an underlying mesh (Φ) with n_x, n_y, and n_z control points along x, y and z direction, respectively. The control-points displacement is computed minimizing a cost function based on the distance ($d(M,F)$) between M and F:

$$d(M,F) = \sum_{\vec{m}\in M} \min_{\vec{f}\in F} \|\vec{f} - \vec{m}\|^2 \tag{1}$$

Here, the $d(M,F)$ was minimized with the Levenberg-Marquardt optimization algorithm [16].

The displacement of a generic point $\vec{m} \in M$ with coordinates (x,y,z) was computed using a B-spline interpolation kernel:

$$T(x,y,z) = \sum_{l=0}^{3}\sum_{m=0}^{3}\sum_{n=0}^{3} B_l(u)B_m(v)B_n(w)\phi_{i+l,j+m,k+n}. \tag{2}$$

where $i = |x/n_x| - 1$, $j = |y/n_y| - 1$, $k = |z/n_z| - 1$, $u = x/n_x - |x/n_x|$, $v = y/n_y - |y/n_y|$, $w = z/n_z - |z/n_z|$, and where $B_l(u)$, $B_m(v)$, $B_n(w)$ are the spline basis functions:

$$B_0(u) = \frac{(1-u)^3}{6}, \tag{3}$$

$$B_1(u) = \frac{3u^3 - 6u^2 + 4}{6}, \tag{4}$$

$$B_2(u) = \frac{-3u^3 + 3u^2 + 3u + 1}{6}, \tag{5}$$

$$B_3(u) = \frac{u^3}{6}. \tag{6}$$

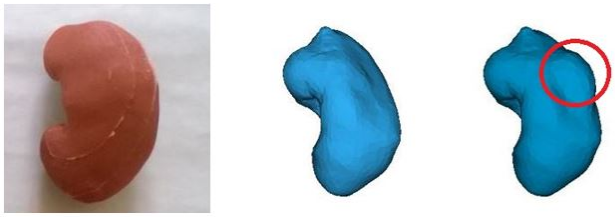

Fig. 3: (Left) Kidney silicon phantom obtained from pre-operative CT scans. (Center) 3D kidney model and (right) manually-deformed model exploited to test the registration algorithm experimentally. The deformed region is highlighted by the red circle.

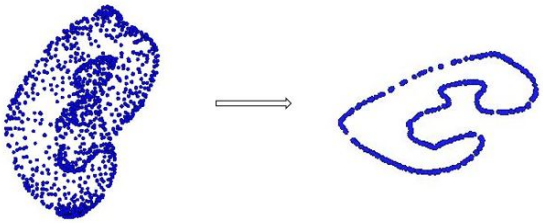

Fig. 4: (Left) 3D point cloud and (right) 2D point cloud obtained by projecting the 3D cloud on a plane and retrieving only the edges.

The spline basis functions are known for a given $\vec{m}$, and weight the contribution of each $\phi_{i,j,k}$ to $T(\vec{m})$ considering the distance between the point $\vec{m}$ and $\phi_{i,j,k}$.

III. Experimental protocol

In this work, the kidney model was obtained from the anonymized Ircadb2 dataset[4]. The Ircadb2 dataset contains an abdominal CT volume of a male patient, acquired with 512x512x167 resolution and voxel size of 0.961x0.961x1.8 mm. Fig. 3 shows the kidney silicon phantom (left) and 3D model (center).

To test FFD in a controlled environment, first 10 artificial F were obtained by manually deforming M with Blender[5], a free and open source 3D creation suite. The deformation replicated tissue-surgical tool interactions, such as tissue manipulation. Fig. 3 (right) shows an example of applied deformation. FFD performance was tested also in the 2D case. The 2D tests were performed on the kidney boundaries, which were obtained by projecting M on a 2D plane and retrieving the cloud edges, as shown in Fig. 4. Also for the 2D case, 10 deformation were applied on the 2D cloud. In both cases, the maximum allowed number of FFD iterations (max_{iter}) was 10000.

To evaluate the registration-algorithm performances, the Root Mean Square Error (RMSE) reduction before and after the registration ($-\Delta_{RMSE}$) was used:

$$-\Delta_{RMSE} = \frac{RMSE_{initial} - RMSE_{final}}{RMSE_{initial}} \quad (7)$$

[4]https://www.ircad.fr/research/3d-ircadb-02/

[5]https://www.blender.org/

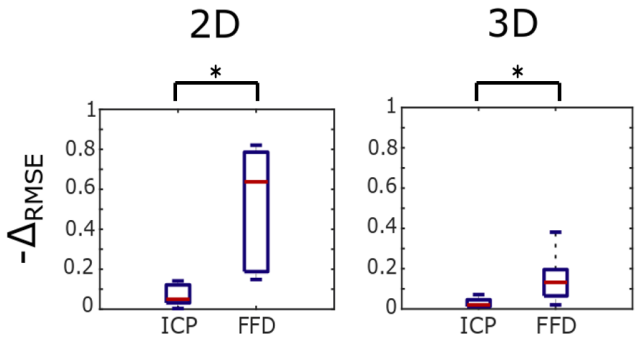

Fig. 5: Root Mean Square Error (RMSE) reduction ($-\Delta_{RMSE}$) after registration. The $-\Delta_{RMSE}$, computed for all model points $\vec{m} \in M$, is reported for 2D and 3D registration for Iterative Closest Point (ICP) and Free Form Deformation (FFD).

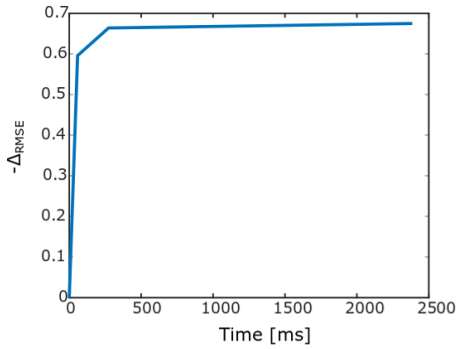

Fig. 6: Root Mean Square Error (RMSE) reduction ($-\Delta_{RMSE}$) after registration vs computational time. Results are relative to Free Form Deformation (FFD) registration

where $RMSE = \sqrt{d(M,F)}$.

The performance of FFD were compared with the performance of a rigid registration algorithm, the Iterative Closest Point (ICP) [17]. The $-\Delta_{RMSE}$ obtained for ICP and FFD were compared using the Wilcoxon test with $\alpha = 0.05$ to assess whether significant differences existed.

From one of the 10 deformed M in 2D, we evaluated how FFD $-\Delta_{RMSE}$ varied according to max_{iter} = (1,10,100,1000,10000) and we measured the computational time required by the FFD algorithm.

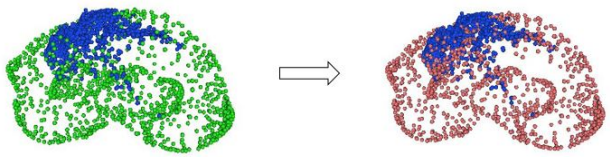

Fig. 7: (Left) Pre-operative kidney model (green) and intra-operative point cloud acquired on silicon phantom (blue). (Right) Deformed pre-operative model (red) after registration with free form deformation.

TABLE I: ROOT MEAN SQUARE ERROR (RMSE) WITH INCREASING DEFORMATION AMPLITUDE

$RMSE_{initial}$ *(mm)*	$RMSE_{final,FFD}$ *(mm)*	$-\Delta_{RMSE}$
0.34	0.29	0.13
0.53	0.33	0.37
0.56	0.33	0.41
0.65	0.34	0.47
0.74	0.46	0.38
0.87	0.37	0.58

Initial ($RMSE_{initial}$) RMSE and RMSE after free form deformation ($RMSE_{final}$) are reported for the 2D case. The RMSE reduction ($-\Delta_{RMSE}$) is reported, too.

The FFD was finally tested for registering the kidney model on real intra-operative point cloud, which was obtained by acquiring phantom images and performing 3D reconstruction as in **Calibration and 3D reconstruction**.

IV. Results

The ICP and FFD $-\Delta_{RMSE}$ for the 2D and 3D cases boxplots are shown in Fig. 5. For the 2D case, median $-\Delta_{RMSE}$ was 0.05 (with interquartile range (IQR) of 0.09) and 0.64 (IQR = 0.60) for ICP and FFD, respectively. For the 3D case, median $-\Delta_{RMSE}$ was 0.02 (IQR = 0.03) for ICP and 0.13 (IQR = 0.13) for FFD. Significant differences were found when comparing ICP and FFD both for the 2D and 3D case. The values of $-\Delta_{RMSE}$ when max_{iter} was changed in (1,10,100,1000,10000) are shown in Fig. 6. In particular, the time required by the FFD registration is reported. The $-\Delta_{RMSE}$ for the 6 manually deformed F with increasing deformation amplitude is shown in Tab. I. The results of the FFD registration on real phantom point cloud are shown in Fig. 7.

V. Discussion and conclusion

With our experimental protocol, FFD provided a more accurate registration than ICP with statistical evidence. The relation between computational time and $-\Delta_{RMSE}$ suggested that stopping FFD after few iterations can be a good solution to achieve a trade-off between computational time and registration accuracy. The results in Tab. I shows that FFD is robust to different level of deformation. The visual analysis of the registration outcome in Fig. 7 showed that the registration was successfully performed also with real point cloud.

As future work, to further automatize the registration process, we aim at exploiting strategies for the automatic intra-operative point-cloud segmentation, as to identify automatically which are the corresponding regions to be registered [18]. To conclude, this work can be also exploited as a promising strategy towards the automatic identification of AC in AR systems for nephrectomy.

Acknowledgement

This work was partially funded by the European Union's Horizon 2020 research and innovation programme under grant agreement No 732515 (SMARTsurg).

References

[1] M. Crundwell, "Pathology and genetics of tumours of the urinary system and male genital organs," *Bju International*, vol. 94, no. 4, pp. 675–675, 2004.

[2] T. M. Fullum, J. A. Ladapo, B. J. Borah, and C. L. Gunnarsson, "Comparison of the clinical and economic outcomes between open and minimally invasive appendectomy and colectomy: evidence from a large commercial payer database," *Surgical Endoscopy*, vol. 24, no. 4, pp. 845–853, 2010.

[3] G. Dogangil, B. Davies, and F. Rodriguez y Baena, "A review of medical robotics for minimally invasive soft tissue surgery," *Proceedings of the Institution of Mechanical Engineers, Part H: Journal of Engineering in Medicine*, vol. 224, no. 5, pp. 653–679, 2010.

[4] S. Nicolau, L. Soler, D. Mutter, and J. Marescaux, "Augmented reality in laparoscopic surgical oncology," *Surgical oncology*, vol. 20, no. 3, pp. 189–201, 2011.

[5] S. Moccia, E. De Momi, S. El Hadji, and L. S. Mattos, "Blood vessel segmentation algorithms–Review of methods, datasets and evaluation metrics," *Computer Methods and Programs in Biomedicine*, vol. 158, pp. 71–91, 2018.

[6] S. Bernhardt, S. A. Nicolau, L. Soler, and C. Doignon, "The status of augmented reality in laparoscopic surgery as of 2016," *Medical image analysis*, vol. 37, pp. 66–90, 2017.

[7] A. Hughes-Hallett, E. K. Mayer, H. J. Marcus, T. P. Cundy, P. J. Pratt, A. W. Darzi, and J. A. Vale, "Augmented reality partial nephrectomy: examining the current status and future perspectives," *Urology*, vol. 83, no. 2, pp. 266–273, 2014.

[8] Y. Gao, R. Kikinis, S. Bouix, M. Shenton, and A. Tannenbaum, "A 3d interactive multi-object segmentation tool using local robust statistics driven active contours," *Medical image analysis*, vol. 16, no. 6, pp. 1216–1227, 2012.

[9] J. A. Sethian, "Fast marching methods," *SIAM review*, vol. 41, no. 2, pp. 199–235, 1999.

[10] V. Penza, J. Ortiz, L. S. Mattos, A. Forgione, and E. De Momi, "Dense soft tissue 3d reconstruction refined with super-pixel segmentation for robotic abdominal surgery," *International journal of computer assisted radiology and surgery*, vol. 11, no. 2, pp. 197–206, 2016.

[11] V. Penza, A. Ciullo, S. Moccia, L. Mattos, and E. De Momi, "Endoabs dataset: Endoscopic abdominal stereo image dataset for benchmarking 3d stereo reconstruction algorithms," *The International Journal of Medical Robotics and Computer Assisted Surgery*, under minor revision.

[12] T. W. Sederberg and S. R. Parry, "Free-form deformation of solid geometric models," *ACM SIGGRAPH computer graphics*, vol. 20, no. 4, pp. 151–160, 1986.

[13] S. Kabus, T. Netsch, B. Fischer, and J. Modersitzki, "B-spline registration of 3d images with levenberg-marquardt optimization," in *Medical Imaging 2004: Image Processing*, vol. 5370. International Society for Optics and Photonics, 2004, pp. 304–314.

[14] D. Khodadad, A. Ahmadian, M. Ay, A. F. Esfahani, H. Y. Banaem, and H. Zaidi, "B-spline based free form deformation thoracic non-rigid registration of ct and pet images," in *International Conference on Graphic and Image Processing (ICGIP 2011)*, vol. 8285. International Society for Optics and Photonics, 2011, p. 82851K.

[15] D. Mattes, D. R. Haynor, H. Vesselle, T. K. Lewellen, and W. Eubank, "Pet-ct image registration in the chest using free-form deformations," *IEEE transactions on medical imaging*, vol. 22, no. 1, pp. 120–128, 2003.

[16] K. Levenberg, "A method for the solution of certain non-linear problems in least squares," *Quarterly of applied mathematics*, vol. 2, no. 2, pp. 164–168, 1944.

[17] P. J. Besl, N. D. McKay *et al.*, "A method for registration of 3-d shapes," *IEEE Transactions on pattern analysis and machine intelligence*, vol. 14, no. 2, pp. 239–256, 1992.

[18] S. Moccia, S. J. Wirkert, H. Kenngott, A. S. Vemuri, M. Apitz, B. Mayer, E. De Momi, L. Mattos, and L. Maier-Hein, "Uncertainty-aware organ classification for surgical data science applications in laparoscopy," *Transactions on Biomedical Engineering*, Accepted for publication.